Integration of Centralized and Distributed Methods to Mitigate Voltage Unbalance Using Solar Inverters

Kshitij Girigoudar, *Member, IEEE*, Mengqi Yao, *Member, IEEE*, Johanna L. Mathieu, *Senior Member, IEEE*, and Line A. Roald, *Member, IEEE*

***Abstract*—Growing penetrations of single-phase distributed generation such as rooftop solar photovoltaic (PV) systems can increase voltage unbalance in distribution grids. However, PV systems are also capable of providing reactive power compensation to reduce unbalance. In this paper, we compare two methods to mitigate voltage unbalance with solar PV inverters: a centralized optimization-based method utilizing a three-phase optimal power flow formulation and a distributed approach based on Steinmetz design. While the Steinmetz-based method is computationally simple and does not require extensive communication or full network data, it generally leads to less unbalance improvement and more voltage constraint violations than the optimization-based method. In order to improve the performance of the Steinmetz-based method without adding the full complexity of the optimization-based method, we propose an integrated method that incorporates design parameters computed from the set-points generated by the optimization-based method into the Steinmetz-based method. We test and compare all methods on a large three-phase distribution feeder with time-varying load and PV data. The simulation results indicate trade-offs between the methods in terms of computation time, voltage unbalance reduction, and constraint violations. We find that the integrated method can provide a good balance between performance and information/communication requirements.**

***Index Terms*—Reactive power compensation, solar PV, Steinmetz design, three-phase optimal power flow, voltage unbalance.**

I. Introduction

DEPLOYMENTS of distributed energy resources (DERs) such as rooftop solar photovoltaic (PV) installations are growing. Uncertainty in solar PV generation, which is generally distributed unevenly between phases [1], as well as large, time-varying single-phase loads such as electric vehicles can increase voltage unbalance in distribution grids. Voltage unbalance captures the degree to which the three-phase voltage magnitudes differ between phases and the phase shift deviates from 120 degrees. Unbalanced voltages may lead to damage or derating of three-phase motors [2] and can induce neutral currents in four-wire systems, which increase network losses and affect protection devices [3]. We note that managing voltage unbalance is different from voltage regulation, which only manages voltage magnitudes, e.g., through volt-var control [4], [5], [6], [7].

Inverter-based reactive power control has been proposed as a promising solution to mitigate unbalance since it has lower investment costs and better transient performance [8] than traditional methods, which include balancing DER connections between phases [9]; utilizing switching devices such as transformer tap changers, voltage regulators, and capacitors [10]; or installing static synchronous compensators [11]. Centralized methods that solve a three-phase optimal power flow (OPF) problem using active and/or reactive power injections by inverters as control variables have been discussed in [8], [12], [13], [14], [15]. A major challenge with such centralized optimization-based methods is the computational burden for large systems along with the need for accurate network measurements and reliable communication. Alternatively, distributed optimization methods, such as [4], [5], [16], [17], [18], can be used to reduce the computational burden. However, these methods focus on voltage regulation and cannot be used to accurately capture voltage unbalance because they employ convex relaxations or linear approximations that assume that the distribution grid is nearly balanced. Other distributed or decentralized methods that do not solve any optimization problem and rely on local measurements have been proposed in [19], [20], [21]. These methods are computationally faster and require less sensing and communication, but provide sub-optimal performance compared to optimization-based approaches. The newest distributed/decentralized approaches use data-driven learning to mitigate unbalance. For example, a reinforcement learning approach to volt/var and volt/watt control of PV inverters to mitigate cyber-physical attacks that induce unbalance was proposed in [22]. However, such approaches can require significant data and long training times.

In this paper, we examine and develop methods to mitigate voltage unbalance in distribution grids. Rather than proposing

Manuscript received 7 November 2021; revised 5 April 2022 and 21 September 2022; accepted 8 October 2022. Date of publication 12 October 2022; date of current version 21 April 2023. This work was supported in part by the U.S. DoE's Office of Energy Efficiency and Renewable Energy under Solar Energy Technologies Office under Agreement 34235, and in part by NSF under Grant ECCS-1845093. Paper no. TSG-01781-2021. *(Kshitij Girigoudar and Mengqi Yao contributed equally to this work.) (Corresponding author: Kshitij Girigoudar.)*

Kshitij Girigoudar and Line A. Roald are with the Department of Electrical and Computer Engineering, University of Wisconsin-Madison, Madison, WI 53715 USA (e-mail: girigoudar@wisc.edu; roald@wisc.edu).

Mengqi Yao and Johanna L. Mathieu are with the Department of Electrical Engineering and Computer Science, University of Michigan-Ann Arbor, Ann Arbor, MI 48103 USA (e-mail: mqyao@umich.edu; jlmath@umich.edu).

Color versions of one or more figures in this article are available at https://doi.org/10.1109/TSG.2022.3214192.

Digital Object Identifier 10.1109/TSG.2022.3214192

1949-3053 © 2022 IEEE. Personal use is permitted, but republication/redistribution requires IEEE permission.
See https://www.ieee.org/publications/rights/index.html for more information.

Authorized licensed use limited to: University of Michigan Library. Downloaded on September 24,2023 at 18:35:06 UTC from IEEE Xplore. Restrictions apply.

an optimization-based method or a distributed method, we propose to *integrate both types of methods*. There are few works in the existing literature that focus on integrating different approaches for unbalanced distribution grids. Hierarchical control strategies which integrate centralized and distributed approaches for voltage regulation have been proposed in [4], [6], [7], [18]. However, these strategies also assume that the distribution grid is balanced or nearly balanced, making them unsuitable for mitigating voltage unbalance. Here, to develop an accurate integrated method for unbalanced networks, we first compare the centralized and distributed methods to gain a better understanding of the advantages and limitations of each method and then identify different ways to integrate them in a realistic setting. Specifically, we propose to solve the centralized optimization-based method less frequently and modify the design of the distributed method to incorporate information/set-points generated by the optimization-based method. There are multiple ways in which the optimization-based set-points can be leveraged in the distributed method, and hence an important contribution of our paper is to assess which integration approach is most promising. Our ultimate goal is to achieve similar performance as the centralized optimization-based method, but with requirements on computation, sensing, and communication that are comparable to that of the distributed method.

The centralized optimization-based method used in this paper determines inverter set-points by solving the three-phase OPF problem proposed in [15], which we solve here with a successive linearization approach to improve computation time. This method achieves the best possible solutions while satisfying all network constraints, but requires full knowledge of the system and extensive communication infrastructure to collect the real-time load and PV generation at every single node in the system. The distributed method is based on [21] and computes inverter set-points by solving a system of linear equations based on Steinmetz design [23]. This method only requires local measurements of the voltage at and the power flowing into one or more nodes and a simple one-way communication network to send commands to inverters. Relative to [21], the Steinmetz-based method is extended to further reduce unbalance as well as voltage constraint violations.

While theoretical guarantees and convergence proofs are important for establishing performance, they are notoriously hard to obtain for realistic power system problems. Therefore, we leave this to future work and instead focus here on investigating performance empirically but rigorously using highly-realistic simulations. Moreover, we identify conditions under which the centralized, distributed, and integrated methods are suitable or not suitable to be implemented in practice.

The main contributions of this paper are as follows. 1) We review the previously-developed optimization-based [15] and Steinmetz-based [21] methods, and identify the pros and cons of each method. Relative to [21], we extend the Steinmetz-based method to further reduce unbalance as well as voltage constraint violations. 2) We identify different ways in which the two approaches can be integrated to achieve the benefits of both methods. Specifically, we discuss various ways in which the infrequently obtained set-points from the optimization-based method can be leveraged by the Steinmetz-based approach. 3) We compare the performance of the previously-developed optimization-based and Steinmetz-based methods as well as six variations of the integrated method in simulations on a large, realistic distribution feeder with time-varying realistic PV generation and residential load data. Specifically, we compare unbalance reduction, voltage constraint violations, and computational time for each method, considering different computation and communication delays. 4) Based on the simulation results, we quantify the advantages and drawbacks of each method and identify the most promising integrated approach which we refer to as the direct implementation approach with local PV strategy. Our results demonstrate that this integrated approach outperforms the optimization-based and Steinmetz-based methods.

The rest of the paper is structured as follows. Section II introduces the voltage unbalance problem and the challenges associated with the optimization-based and Steinmetz-based methods. Section III details both methods and introduces the design of the integrated method. Section IV presents a case study that explores the performance of each method on a large taxonomic feeder using actual PV generation and residential load data. Section V concludes the paper.

II. Voltage Unbalance Problem and Challenges

In this section, we first define unbalance and then provide a high-level overview of the voltage unbalance problem and two existing methods to address it.

We use the voltage unbalance definition adopted by IEC Standard 61000-2-2 [24] and commonly referred to as the Voltage Unbalance Factor (VUF). In phasor notation $V = |V|\angle\theta$, where V is a complex voltage phasor, $|V|$ is the voltage magnitude, and θ is the voltage angle. The complex conjugate of V is denoted by V^*. For a three-phase node i, the VUF is

$$\begin{aligned} \text{VUF}_i\ [\%] &= \frac{|V_i^-|}{|V_i^+|} \times 100, \quad \text{where} \\ V_i^+ &= \frac{V_i^a + \mathrm{a} \cdot V_i^b + \mathrm{a}^2 \cdot V_i^c}{3}, \\ V_i^- &= \frac{V_i^a + \mathrm{a}^2 \cdot V_i^b + \mathrm{a} \cdot V_i^c}{3}. \end{aligned} \tag{1}$$

Here, V_i^+ and V_i^- are the positive and negative sequence voltage phasors [25]; V_i^a, V_i^b, V_i^c are the line-to-neutral voltage phasors at node i, and $\mathrm{a} = 1\angle 120°$. The IEC Standard [24] limits voltage unbalance in low- and medium-voltage systems to 2%. Voltage unbalance causes significant damage to three-phase motors [26], [27], such as temperature rise, output power and torque reduction, and increased losses. As reported in [28], each 0.2% increase in unbalance reduces motor lifetime by approximately one year. Repair and replacement costs due to voltage unbalance are significant, up to $28 billion a year [29]. Therefore, to extend the lifetime of three-phase equipment, we attempt to reduce the VUF at **critical nodes**, i.e., nodes with expensive three-phase equipment (e.g., motors used seasonally at rural farms that do not have reactive power compensation installed.) We do this by controlling the reactive power injections of PV systems without curtailing their active power

Authorized licensed use limited to: University of Michigan Library. Downloaded on September 24,2023 at 18:35:06 UTC from IEEE Xplore. Restrictions apply.

TABLE I
QUALITATIVE COMPARISON OF OPTIMIZATION-BASED AND STEINMETZ-BASED METHODS

	Optimization-based Method	Steinmetz-based Method
Performance	+ Achieves lowest possible VUF at any three-phase node + Cost function can include multiple objectives, such as reducing network losses or unbalance at multiple nodes + Considers network constraints	− Achieves considerable VUF reduction in general cases − Cannot significantly improve VUF with high unbalance upstream of critical node and/or limited downstream reactive power capacity − Does not consider network constraints
Information	− Requires detailed network model − Requires load and PV measurements at every node	+ Does not require network model + Requires only local measurements
Communication	− Requires two-way communication system	+ Requires only one-way communication system
Computation	− Computationally heavy (solves a nonlinear, non-convex optimization problem)	+ Computationally simple (solves a linear system of equations)

injections so that customer energy cost savings or profits are not affected. Our methods can target one or more critical nodes. We also note that mitigating unbalance at just one critical node usually achieves significant unbalance reduction across the entire feeder, as we will show in our case study results in Section IV.

The **optimization-based** method solves a three-phase OPF problem that minimizes the VUF at critical nodes to determine the optimal reactive power injections of PV systems [15]. This method requires a detailed network model (including topology and parameters) as well as load and PV measurements throughout the network. The benefits of this method include its ability to provide the lowest possible voltage unbalance at the critical node, while satisfying all network constraints. However, the drawbacks are the need for accurate system data along with frequent two-way communication to receive measurements from every node and send the reactive power set-points to individual PV systems. Moreover, significant computational effort is required to solve the OPF problem.

The **Steinmetz-based** method utilizes Steinmetz design [23], [30] to calculate the reactive power injections at each critical node that would make the load downstream of that critical node appear balanced. Our previous work [21] extended this approach to instead calculate the change in reactive power injections of PV systems distributed downstream of critical nodes. This method only requires local measurements such as the three-phase complex voltage at each critical node as well as the three-phase complex power flowing into that critical node. Set-points are sent from each critical node through a one-way communication network to the downstream PV systems. The complexity of the Steinmetz-based method is similar to that of a simple local Q-V droop controller used for voltage regulation in that local measurements are used to make decisions on reactive power injections. However, it is different in that it mitigates voltage unbalance through a control policy derived from network physics without the need for heuristic droop coefficients. The Steinmetz-based method requires less sensing, communication, and computational effort than the optimization-based method, but it does not guarantee optimal performance or constraint satisfaction. Furthermore, it does not work well when the unbalance upstream of the critical node is significant and/or the downstream flexible reactive power capacity is limited.

Table I provides a qualitative comparison of the optimization-based and Steinmetz-based methods. We observe that both methods have different advantages and limitations. The key question we address in this paper is whether it is possible to obtain set-points for the PV systems at more frequent intervals than the optimization-based method can provide while also achieving a larger reduction in unbalance and constraint violations than the Steinmetz-based method is able to achieve by itself. To do this, we develop an **integrated** method that can achieve similar performance to the optimization-based method but requires similar communication, measurements, and computation effort as the Steinmetz-based method. The different ways of integration are discussed in Section III. Our case study in Section IV compares all the methods quantitatively.

III. METHODS TO MITIGATE VOLTAGE UNBALANCE

In this section, we describe the optimization-based and Steinmetz-based methods and introduce the integrated method. For ease of exposition, our formulations assume all PV systems are single-phase and connected phase-to-neutral, though our approaches can be easily extended to handle phase-to-phase connected PV systems, as we considered in [15], [21].

A. Optimization-Based Method

The optimization-based method is formulated as a three-phase OPF problem that minimizes voltage unbalance at the critical node. We first provide an overview of the general procedure detailed in our previous work [15]. We then describe how a successive linearization approach can be used to solve the problem.

1) General Procedure: The distribution system is modeled in the phase frame [31]. We consider a radial network where $\mathcal{N}$ is the set of nodes and Ω_{PV} is the set of controllable PV systems. All vectors and matrices are denoted with bold letters. The per-unit voltage magnitudes and angles at any three-phase node i are represented using $|\mathbf{V}_i| = [|V_i^a| \;\; |V_i^b| \;\; |V_i^c|]^\top$ and $\boldsymbol{\theta}_i = [\theta_i^a \;\; \theta_i^b \;\; \theta_i^c]^\top$, respectively. Similarly, the three-phase

Authorized licensed use limited to: University of Michigan Library. Downloaded on September 24,2023 at 18:35:06 UTC from IEEE Xplore. Restrictions apply.

active and reactive power injections at node i are denoted $\mathbf{P}_i = [P_i^a \;\; P_i^b \;\; P_i^c]^\top$ and $\mathbf{Q}_i = [Q_i^a \;\; Q_i^b \;\; Q_i^c]^\top$, respectively. For any single- or two-phase node i, we ignore the missing phases, i.e., $|\mathbf{V}_i|, \boldsymbol{\theta}_i, \mathbf{P}_i, \mathbf{Q}_i \in \mathbb{R}^{n_{\Phi,i}}$ where $n_{\Phi,i}$ is the number of phases at node i. The overall number of single-phase connections is denoted by $n = \sum_{i\in\mathcal{N}} n_{\Phi,i}$.

The distribution substation node 'ref' is assumed to be a perfectly balanced three-phase node and is chosen as the voltage magnitude base and angle reference, i.e.,

$$\mathbf{V}_{\text{ref}} = \begin{bmatrix} 1\angle 0^\circ & \text{a}^2 & \text{a} \end{bmatrix}^\top. \tag{2}$$

We limit all other voltage magnitudes

$$\underline{V} \le |V_i^\phi| \le \overline{V}, \;\; \forall \phi \in \{a,b,c\}, \;\; i \in \mathcal{N} \setminus \text{ref}, \tag{3}$$

where $\underline{V}$ and $\overline{V}$ are the lower and upper per-unit voltage magnitude limits, respectively.

The decision variables are the per-unit reactive power injections of each PV system k denoted $Q_{\text{PV},k}$. We do not curtail its active power injection $P_{\text{PV},k}$, which is assumed known. The PV system reactive power injection is constrained by

$$-\overline{Q}_{\text{PV},k} \le Q_{\text{PV},k} \le \overline{Q}_{\text{PV},k}, \;\; \forall k \in \Omega_{\text{PV}}. \tag{4}$$

Here, $\overline{Q}_{\text{PV},k} = \sqrt{|S_{\text{PV},k}|^2 - (P_{\text{PV},k})^2}$ is the time-varying reactive power capacity of PV system k, which is a function of the time-varying active power injection $P_{\text{PV},k}$ and the fixed rated apparent power $|S_{\text{PV},k}|$.

Set $\Omega_{\text{PV},i}^\phi$ includes PV systems at node $i \in \mathcal{N}$ connected to phase $\phi \in \{a,b,c\}$. The active power injection P_i^ϕ and reactive power injection Q_i^ϕ at $i \in \mathcal{N} \setminus \text{ref}$ are

$$P_i^\phi = \sum_{k\in\Omega_{\text{PV},i}^\phi} P_{\text{PV},k} - P_{\text{L},i}^\phi, \tag{5a}$$

$$Q_i^\phi = \sum_{k\in\Omega_{\text{PV},i}^\phi} Q_{\text{PV},k} - Q_{\text{L},i}^\phi, \tag{5b}$$

where $P_{\text{L},i}^\phi, Q_{\text{L},i}^\phi$ are the active and reactive power demand, respectively. At node 'ref', we need to include the active and reactive power from the substation at phase ϕ, denoted P_{ss}^ϕ and Q_{ss}^ϕ, respectively. The power injections at node 'ref' are

$$P_{\text{ref}}^\phi = P_{\text{ss}}^\phi + \sum_{k\in\Omega_{\text{PV,ref}}^\phi} P_{\text{PV},k} - P_{\text{L,ref}}^\phi, \tag{6a}$$

$$Q_{\text{ref}}^\phi = Q_{\text{ss}}^\phi + \sum_{k\in\Omega_{\text{PV,ref}}^\phi} Q_{\text{PV},k} - Q_{\text{L,ref}}^\phi. \tag{6b}$$

The active power demand $P_{\text{L},i}^\phi$ and reactive power demand $Q_{\text{L},i}^\phi$ at node $i \in \mathcal{N}$ connected to phase $\phi \in \{a,b,c\}$ are modeled as functions of the voltage magnitude using a polynomial (ZIP) load model [32],

$$P_{\text{L},i}^\phi = P_{\text{P},i}^\phi + P_{\text{I},i}^\phi \cdot |V_i^\phi| + P_{\text{Z},i}^\phi \cdot |V_i^\phi|^2, \tag{7a}$$

$$Q_{\text{L},i}^\phi = Q_{\text{P},i}^\phi + Q_{\text{I},i}^\phi \cdot |V_i^\phi| + Q_{\text{Z},i}^\phi \cdot |V_i^\phi|^2, \tag{7b}$$

where $P_{\text{P},i}^\phi + jQ_{\text{P},i}^\phi$ represents the constant power load component, $P_{\text{I},i}^\phi + jQ_{\text{I},i}^\phi$ the constant current load component, and $P_{\text{Z},i}^\phi + jQ_{\text{Z},i}^\phi$ the constant impedance load component.

Following [15], we denote the element-wise product by $\odot$ and express the multi-phase active power injection $\mathbf{P}_i \in \mathbb{R}^{n_{\Phi,i}}$ and reactive power injection $\mathbf{Q}_i \in \mathbb{R}^{n_{\Phi,i}}$ at node $i \in \mathcal{N}$ as

$$\mathbf{P}_i = |\mathbf{V}_i| \odot \sum_{j\in\mathcal{N}} \left[\mathbf{G}_{ij} \odot \mathrm{C}(\boldsymbol{\theta}_{ij}) + \mathbf{B}_{ij} \odot \mathrm{S}(\boldsymbol{\theta}_{ij})\right] \cdot |\mathbf{V}_j|, \tag{8a}$$

$$\mathbf{Q}_i = |\mathbf{V}_i| \odot \sum_{j\in\mathcal{N}} \left[\mathbf{G}_{ij} \odot \mathrm{S}(\boldsymbol{\theta}_{ij}) - \mathbf{B}_{ij} \odot \mathrm{C}(\boldsymbol{\theta}_{ij})\right] \cdot |\mathbf{V}_j|, \tag{8b}$$

where $\mathbf{G}_{ij}, \;\mathbf{B}_{ij} \in \mathbb{R}^{n_{\Phi,i}\times n_{\Phi,j}}$ are submatrices denoting the real and imaginary components of the bus admittance matrix $\mathbf{Y} \in \mathbb{R}^{n\times n}$ derived in [15]. For a branch connecting three-phase nodes i and j, $\mathrm{C}(\boldsymbol{\theta}_{ij}), \;\mathrm{S}(\boldsymbol{\theta}_{ij}) \in \mathbb{R}^{3\times 3}$ are defined as

$$\mathrm{C}(\boldsymbol{\theta}_{ij}) = \begin{bmatrix} \cos\left(\theta_i^a - \theta_j^a\right) & \cos\left(\theta_i^a - \theta_j^b\right) & \cos\left(\theta_i^a - \theta_j^c\right) \\ \cos\left(\theta_i^b - \theta_j^a\right) & \cos\left(\theta_i^b - \theta_j^b\right) & \cos\left(\theta_i^b - \theta_j^c\right) \\ \cos\left(\theta_i^c - \theta_j^a\right) & \cos\left(\theta_i^c - \theta_j^b\right) & \cos\left(\theta_i^c - \theta_j^c\right) \end{bmatrix},$$

$$\mathrm{S}(\boldsymbol{\theta}_{ij}) = \begin{bmatrix} \sin\left(\theta_i^a - \theta_j^a\right) & \sin\left(\theta_i^a - \theta_j^b\right) & \sin\left(\theta_i^a - \theta_j^c\right) \\ \sin\left(\theta_i^b - \theta_j^a\right) & \sin\left(\theta_i^b - \theta_j^b\right) & \sin\left(\theta_i^b - \theta_j^c\right) \\ \sin\left(\theta_i^c - \theta_j^a\right) & \sin\left(\theta_i^c - \theta_j^b\right) & \sin\left(\theta_i^c - \theta_j^c\right) \end{bmatrix}.$$

For single- or two-phase nodes, the missing phase entries are removed, i.e., $\mathrm{C}(\boldsymbol{\theta}_{ij}), \;\mathrm{S}(\boldsymbol{\theta}_{ij}) \in \mathbb{R}^{n_{\Phi,i}\times n_{\Phi,j}}$.

We minimize voltage unbalance at the critical node 'cr' by minimizing the square of VUF_{cr}

$$\min \text{VUF}_{\text{cr}}^2 = \min \frac{|V_{\text{cr}}^-|^2}{|V_{\text{cr}}^+|^2} = \min \frac{{V_{\text{cr,d}}^-}^2 + {V_{\text{cr,q}}^-}^2}{{V_{\text{cr,d}}^+}^2 + {V_{\text{cr,q}}^+}^2}, \tag{9}$$

where $V_{\text{cr,d}}^-, V_{\text{cr,q}}^-$ and $V_{\text{cr,d}}^+, V_{\text{cr,q}}^+$ are the rectangular form representation of the negative and positive sequence voltage phasors V^- and V^+. The subscript 'd' denotes the real part and 'q' denotes the imaginary part. Note that it is easy to include multiple critical nodes in the objective function by summing up the square of the VUF at all of the critical nodes.

In summary, the three-phase OPF is

$$\begin{aligned} \min \;\; & \text{VUF}_{\text{cr}}^2 \\ \text{s.t.} \;\; & \text{Voltage limits: (2), (3),} \\ & \text{Reactive power limits: (4),} \\ & \text{Nonlinear AC power flow: (5)}-\text{(8).} \end{aligned} \tag{10}$$

Other constraints such as branch current limits can be easily included in the three-phase OPF problem formulation. Although branch current limits could become a concern with increasing PV penetrations, we omit these constraints to focus on voltage unbalance problems.

2) Solution Timeframe: The three-phase OPF (10) is nonconvex and nonlinear which makes it challenging to solve for large systems. In practice, it would need to be solved frequently as load and PV generation change. As illustrated in Fig. 1, we assume load and PV measurements are available at regular time intervals τ_{m}. However, the corresponding reactive power set-points are available only after a time delay τ_{d} that includes both the computational time as well as the communication delay associated with acquiring measurements and

Authorized licensed use limited to: University of Michigan Library. Downloaded on September 24,2023 at 18:35:06 UTC from IEEE Xplore. Restrictions apply.

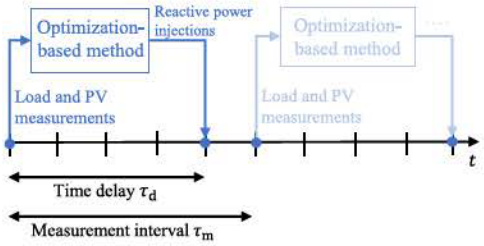

Fig. 1. Optimization-based method implemented on a time-varying system.

sending set-points to the PV systems. If the delay τ_d is large, the reactive power set-points may no longer be optimal since load and especially PV generation can change quickly in real distribution systems.

3) Successive Linearization: In [15], we solved the nonlinear optimization problem (10) with Ipopt. In this paper, to reduce the computation time, we employ a successive linearization approach [33], [34]. In successive linearization, we start with an initial power flow solution, about which we linearize the AC power flow equations using a first-order Taylor series approximation. Then, we embed the approximation in a modified OPF problem that selects the optimal *changes* in the decision variables from the previous power flow solution, and computes the decision variables ($|\mathbf{V}_i|, \theta_i \; \forall i \in \mathcal{N}, Q_{\text{PV},k} \; \forall k \in \Omega_{\text{PV}}$) as the previous solution plus the change. Using these decision variables, we solve the power flow and repeat the process until convergence to an AC feasible solution. The solution has converged when the total deviation of the new solution with respect to the previous solution is below a specified tolerance. For the ZIP load model, we utilize a zero-order approximation by using the initial voltage magnitude solution in (7) to compute the approximate load demand. This is recalculated in each iteration based on the updated voltage solution.

The difference between our approach and the classic successive linearization approach for OPF is that the power flow Jacobian used in the approximation corresponds to the three-phase unbalanced system and is of dimension $\mathbb{R}^{2n\times 2n}$. In addition, we maintain nonlinear expressions for the VUF objective, which means that the problem is still non-convex after the power flow equations have been linearized.

When minimizing the VUF at the critical node(s), the optimization algorithm can sometimes identify solutions that would require large reactive power injections from the PV systems. Such solutions are less desirable than solutions with smaller reactive power injections and, in some cases, they also lead to convergence problems for the algorithm. To promote solutions with moderate reactive power injections and faster convergence, we add a penalty on the reactive power injections to our objective function (9),

$$Q_{\text{pen}} = w \sum_{k\in\Omega_{\text{PV}}} \left(Q_{\text{PV},k}\right)^2. \tag{11}$$

Here, w is a scalar weighting factor, which we choose to be small to ensure that higher priority is given to minimizing VUF. A larger w will reduce the reactive power injections from PV systems and promote convergence of the algorithm, but may also increase the resulting VUF.

B. Steinmetz-Based Method

The Steinmetz-based method computes the change in reactive power injections needed make the load downstream of a critical node appear balanced. We use the distributed controller from [21], which requires a simple communication network. Steinmetz design can also be implemented in a completely decentralized way [21], but this is not discussed here. We first describe the general procedure and then propose two new heuristic strategies that improve performance.

1) General Procedure: First, consider a single critical node. As shown in (1), VUF_{cr} becomes zero when the negative-sequence voltage V_{cr}^- is eliminated. If the network upstream of the critical node is balanced, then V_{cr}^- becomes zero when the negative-sequence current I_{cr}^- is driven to zero. Denote the change in reactive power injections required to make the load downstream of the critical node appear balanced by $\Delta\mathbf{Q}_{\text{cr}} = \left[\Delta Q_{\text{cr}}^a \;\; \Delta Q_{\text{cr}}^b \;\; \Delta Q_{\text{cr}}^c\right]^\top$. To compute $\Delta\mathbf{Q}_{\text{cr}}$ we set the negative-sequence current to zero, i.e.,

$$3I_{\text{cr}}^- = I_{\text{cr}}^a + \text{a}^2 \cdot I_{\text{cr}}^b + \text{a} \cdot I_{\text{cr}}^c = 0, \tag{12}$$

where $I_{\text{cr}}^\phi = ((S_{\text{cr}}^\phi + j\Delta Q_{\text{cr}}^\phi)/V_{\text{cr}}^\phi)^* \; \forall\phi \in \{a,b,c\}$ are the phase currents flowing into the critical node and $S_{\text{cr}}^\phi \; \forall\phi \in \{a,b,c\}$ are the complex power flowing into the critical node (including both the load at the critical node and the total downstream load and line losses), with $\mathbf{S}_{\text{cr}} = \left[S_{\text{cr}}^a \; S_{\text{cr}}^b \; S_{\text{cr}}^c\right]^\top$.

Splitting (12) into its real and imaginary parts, we obtain two equations; however, $\Delta\mathbf{Q}_{\text{cr}}$ has three unknowns. In order to reach a unique solution, we add a constraint that sets the sum of changes in reactive power injections to a specific value $\hat{Q}$, i.e.,

$$\Delta Q_{\text{cr}}^a + \Delta Q_{\text{cr}}^b + \Delta Q_{\text{cr}}^c = \hat{Q}, \tag{13}$$

where $\hat{Q}$ is a design parameter. The change in the three-phase reactive power injections $\Delta\mathbf{Q}_{\text{cr}}$ can now be obtained by solving the system of equations (12) and (13), which we write compactly as

$$\Delta\mathbf{Q}_{\text{cr}} = f\left(\mathbf{S}_{\text{cr}}, \mathbf{V}_{\text{cr}}, \hat{Q}\right), \tag{14}$$

where $\mathbf{V}_{\text{cr}} = \left[V_{\text{cr}}^a \; V_{\text{cr}}^b \; V_{\text{cr}}^c\right]^\top$. In [21], we set $\hat{Q}$ to zero so that the total reactive power demand of the system remained constant and the voltage profile did not change significantly.

We need to assign a share of the total change in reactive power $\Delta\mathbf{Q}_{\text{cr}}$ to each controlled PV system, which we do using

$$\Delta Q_{\text{PV},k} = \gamma_k \Delta Q_{\text{cr}}^\phi, \quad \forall k \in \Omega_{\text{PV,d}}. \tag{15}$$

Here, $\Delta Q_{\text{PV},k}$ is the change in set-point for PV system k, $\gamma_k \in [0,1]$ is the reactive power contribution ratio from PV system k, PV system k is connected to phase ϕ, and $\Omega_{\text{PV,d}}$ is the set of controllable PV systems downstream of the critical node. To ensure the sum of changes in reactive power injections equals $\hat{Q}$, we set

$$\sum_{k\in\Omega_{\text{PV,d}}^\phi} \gamma_k = 1, \quad \forall\phi \in \{a,b,c\}, \tag{16}$$

Authorized licensed use limited to: University of Michigan Library. Downloaded on September 24,2023 at 18:35:06 UTC from IEEE Xplore. Restrictions apply.

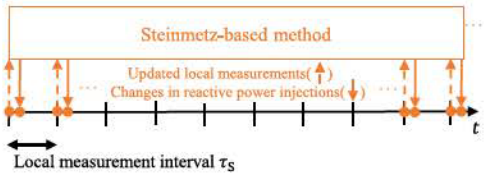

Fig. 2. Steinmetz-based method implemented on a time-varying system.

where $\Omega^{\phi}_{\text{PV,d}}$ is the set of controllable PV systems downstream of the critical node that are connected to phase ϕ. Like $\hat{Q}$, the contribution ratios $\gamma_k\ \forall k \in \Omega_{\text{PV,d}}$ are also design parameters. In [21], we allocated $\Delta\mathbf{Q}_{\text{cr}}$ to each PV system based on its rated apparent power using

$$\gamma_k = \frac{|S_{\text{PV},k}|}{\sum_{k' \in \Omega^{\phi}_{\text{PV,d}}} |S_{\text{PV},k'}|}, \quad \forall k \in \Omega_{\text{PV,d}}. \tag{17}$$

Since $|S_{\text{PV},k}|$ is constant over time, we refer to the contribution ratio computed with (17) as the **constant ratio**.

Each PV system implements the change in reactive power set-point up to their reactive power limits, i.e., at timestep t

$$Q^t_{\text{PV},k} = \begin{cases} \overline{Q}^t_{\text{PV},k}, & \text{if } Q^{t-1}_{\text{PV},k} + \Delta Q^t_{\text{PV},k} > \overline{Q}^t_{\text{PV},k} \\ -\overline{Q}^t_{\text{PV},k}, & \text{if } Q^{t-1}_{\text{PV},k} + \Delta Q^t_{\text{PV},k} < -\overline{Q}^t_{\text{PV},k} \\ Q^{t-1}_{\text{PV},k} + \Delta Q^t_{\text{PV},k}, & \text{otherwise.} \end{cases} \tag{18}$$

When the system has multiple critical nodes, the above process is applied at multiple nodes simultaneously. Each critical node will control downstream PV systems up to the next downstream critical node. In [35], a convergence condition is established for when the feeder has multiple critical nodes.

In [21], we showed that, even if all PV systems exactly implement the requested change in reactive power set-point (15), the system does not become perfectly balanced because downstream losses (i.e., the downstream load imposed by the network itself) will change with the change in reactive power injections. If load and PV generation remained constant over time, reactive power set-point changes could be recomputed with new measurements iteratively until unbalance converged to zero or a small value. In practice, load and PV generation vary over time and so it is not possible to achieve exact convergence. Therefore, we compute the changes in reactive power injections whenever new local measurements of $\mathbf{S}_{\text{cr}}$ and $\mathbf{V}_{\text{cr}}$ are available, e.g., at regular time intervals τ_s as shown in Fig. 2. Since these measurements are gathered locally, the interval τ_s can be much shorter than the interval τ_m used by the optimization-based method. Moreover, the time delay associated with solving the system of equations (14) and sending set-points is so small that it is neglected (i.e., $\tau_d = 0$ for this method).

2) Heuristic Strategies: As discussed in Section II, the Steinmetz-based method does not perform well when unbalance upstream of the critical node is significant and/or downstream flexible reactive power capacity is limited. Furthermore, the method does not consider network constraints and so can lead to voltage magnitude limit violations. We propose two strategies to mitigate these drawbacks.

The first strategy **controls PV systems upstream of the critical node** to help reduce unbalance at the critical node. Specifically, we use upstream PV systems, belonging to the set $\Omega_{\text{PV,u}} = \Omega_{\text{PV}} \setminus \Omega_{\text{PV,d}}$, to balance a proxy critical node near the substation, while using downstream PV systems to balance the critical node. This means that we implement the Steinmetz-based method on two nodes simultaneously, where the controller at the proxy critical node uses only a portion of the downstream PV systems, specifically, those not controlled by the controller at the critical node. This requires one-way communication between the proxy critical node and PV systems in $\Omega_{\text{PV,u}}$, and between the critical code and the PV systems in $\Omega_{\text{PV,d}}$, but no communication between the critical nodes. Note that this approach can be further generalized to an arbitrary number of controllers each controlling a subset of the PV systems downstream of that controller.

The second strategy, referred to as the **local PV strategy**, reduces voltage magnitude limit violations. Since voltage magnitudes and reactive power injections are positively correlated, PV systems use local voltage measurements to modify reactive power set-points that would exacerbate voltage constraint violations using

$$\Delta\widetilde{Q}_{\text{PV},k} = \begin{cases} -\beta\Delta Q_{\text{PV},k}, & \text{if } \left(|V^{\phi}_i| - \underline{V}\right) < 0 \text{ and } \Delta Q_{\text{PV},k} < 0 \\ -\beta\Delta Q_{\text{PV},k}, & \text{if } \left(|V^{\phi}_i| - \overline{V}\right) > 0 \text{ and } \Delta Q_{\text{PV},k} > 0 \\ \Delta Q_{\text{PV},k}, & \text{otherwise,} \end{cases} \tag{19}$$

where PV system k is connected to phase ϕ of node i, and β is a positive scalar. For example, if $|V^{\phi}_i|$ is greater than the upper limit and the controller asks for an increase in reactive power, i.e., $\Delta Q_{\text{PV},k} > 0$, the PV system will instead reduce reactive power to decrease the voltage magnitude, and vice versa when the voltage is less than the lower limit. Here, we simply set $\beta = 1$. In our case study, we discuss the benefits and some drawbacks of this approach.

C. Integrated Method

We next introduce the integrated method, which attempts to achieve the simplicity and speed of the Steinmetz-based method with the performance of the optimization-based method. Specifically, the integrated method uses solutions obtained periodically from the optimization-based method to choose the design parameters $\hat{Q}$ and $\gamma_k, \forall k \in \Omega_{\text{PV,d}}$ used in the Steinmetz-based method. We compute the sum of changes in reactive power injections $\hat{Q}$ from two consecutive optimization-based method solutions, i.e.,

$$\hat{Q}^t = \sum_{k \in \Omega_{\text{PV,d}}} \left(Q^t_{\text{PV},k} - Q^{t-\tau_m}_{\text{PV},k}\right), \tag{20}$$

where $Q^t_{\text{PV},k}$ is the optimal reactive power set-point of PV system k at time t. Note that here we use notation corresponding to the controller at the critical node, but the integrated method can also be used by the controller at the proxy critical node. The contribution ratios $\gamma_k\ \forall k \in \Omega_{\text{PV,d}}$ are set equal to

Authorized licensed use limited to: University of Michigan Library. Downloaded on September 24,2023 at 18:35:06 UTC from IEEE Xplore. Restrictions apply.

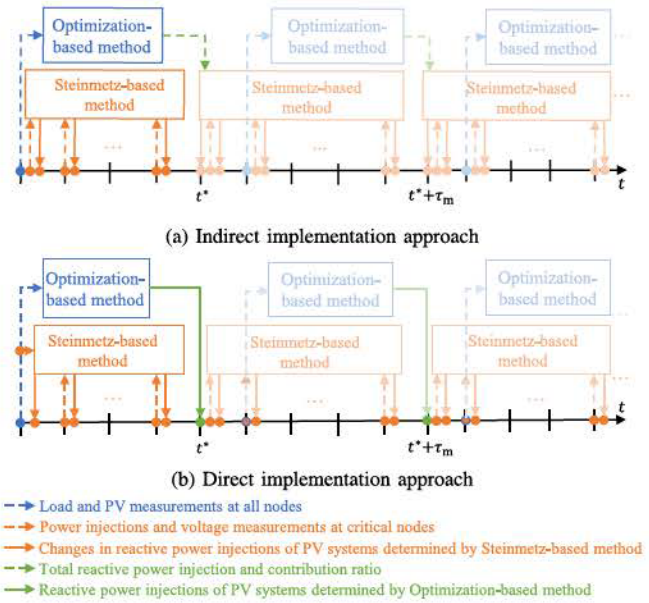

Fig. 3. Two approaches to implementing the integrated method.

the ratios obtained by the optimization-based method

$$\gamma_k^t = \frac{Q_{\mathrm{PV},k}^t}{\sum_{k' \in \Omega_{\mathrm{PV,d}}^{\phi}} Q_{\mathrm{PV},k'}^t}, \quad \forall k \in \Omega_{\mathrm{PV,d}}, \tag{21}$$

which we refer to as the **varying ratio** since it changes over time.

We now introduce two approaches to implementing the integrated method. Fig. 3 shows both approaches.

1) Indirect Implementation Approach: The indirect implementation approach uses the results of the optimization-based method at t^* to compute the change in reactive power injections, i.e.,

$$\Delta \mathbf{Q}_{\mathrm{cr}}^{t^*} = f\left(\mathbf{S}_{\mathrm{cr}}^{t^*}, \mathbf{V}_{\mathrm{cr}}^{t^*}, \sum_{k \in \Omega_{\mathrm{PV,d}}} \left(Q_{\mathrm{PV},k}^{t^*} - Q_{\mathrm{PV},k}^{t^*-\tau_m}\right)\right). \tag{22}$$

Then, until new optimization-based method results are received, we update the reactive power injections using

$$\Delta \mathbf{Q}_{\mathrm{cr}}^{t} = f\left(\mathbf{S}_{\mathrm{cr}}^{t}, \mathbf{V}_{\mathrm{cr}}^{t}, 0\right), \quad \forall t \in \left(t^*, t^* + \tau_m\right), \tag{23}$$

i.e., we do not change the total injected reactive power since we have no further information from the optimization-based method. The indirect implementation approach is shown in Fig. 3(a).

2) Direct Implementation Approach: The direct implementation approach directly applies the reactive power set-points $\mathbf{Q}_{\mathrm{PV}}^{t^*}$ of the optimization-based method when it is available, as shown in Fig. 3(b). Then, until new optimization-based method results are received, the Steinmetz-based method does not attempt to make the entire downstream load appear balanced. Instead, it attempts to make the change in downstream load from the optimal downstream load $\Delta \mathbf{S}_{\mathrm{cr}}^t = \mathbf{S}_{\mathrm{cr}}^t - \mathbf{S}_{\mathrm{cr}}^{t^*}$, where $\mathbf{S}_{\mathrm{cr}}^{t^*}$ is obtained from the optimization-based method at t^*, appear balanced. Therefore, we update the reactive power injections using

$$\Delta \mathbf{Q}_{\mathrm{cr}}^{t} = f\left(\Delta \mathbf{S}_{\mathrm{cr}}^{t}, \mathbf{V}_{\mathrm{cr}}^{t}, 0\right), \quad \forall t \in \left(t^*, t^* + \tau_m\right), \tag{24}$$

where, again, $\hat{Q}^t = 0$ since have no further information from the optimization-based method.

In summary, when using the indirect implementation approach, the Steinmetz-based method obtains set-points from the optimization-based method, performs a calculation to obtain the reactive power injections, and then sends them to the PV systems. In contrast, when using the direct implementation approach, the results from the optimization-based approach are sent directly to the PV systems without any changes. This difference in how the optimization-based solutions are used is shown by the green arrows in Fig. 3. We further note that both the indirect and direct implementation approaches can be combined with either the constant (17) or varying (21) contribution ratios $\gamma_k \ \forall k \in \Omega_{\mathrm{PV}}$.

TABLE II
SUMMARY OF METHODS TO MITIGATE VOLTAGE UNBALANCE

Abbreviation	Method	$\hat{Q}$	γ	Local PV Strategy
OM	Optimization-based	-	-	-
SM	Steinmetz-based	0	Constant	N
$\mathrm{SM_{PV}}$	Steinmetz-based	0	Constant	Y
$\mathrm{InDir_{opt}}$	Integrated: Indirect	OM Results	Varying	N
$\mathrm{InDir_{opt,PV}}$	Integrated: Indirect	OM Results	Varying	Y
$\mathrm{InDir_{cons,PV}}$	Integrated: Indirect	OM Results	Constant	Y
$\mathrm{Dir_{opt}}$	Integrated: Direct	OM Results	Varying	N
$\mathrm{Dir_{opt,PV}}$	Integrated: Direct	OM Results	Varying	Y
$\mathrm{Dir_{cons,PV}}$	Integrated: Direct	OM Results	Constant	Y

D. Method Summary

Table II summarizes all of the methods, and lists the full set of variations that we explore in our case studies. For each variation, we list its abbreviation, the underlying method, how the sum of changes in reactive power injections $\hat{Q}$ is computed, how the contribution ratios γ are computed, and whether (Y) or not (N) the local PV strategy is applied. The optimization-based method does not use $\hat{Q}$, γ, or the local PV strategy. The Steinmetz-based method can be applied with or without the local PV strategy. For the variations on the integrated method all use optimization-based method results (OM Results) to compute $\hat{Q}$, but differ in whether the direct or indirect implementation approach is used, the constant or varying contribution ratio is used for γ, and the local PV strategy is used to manage voltage violations.

IV. CASE STUDY

We next present a case study that compares each of the methods applied to a large feeder. For demonstrations of the performance of the optimization-based and Steinmetz-based methods on small test feeders, we refer interested readers to our previous work in [36] and [21]. We first describe the feeder, simulation implementation, and performance metrics. We then detail results of static and time-varying cases. Finally, we provide recommendations for the most suitable methods under different scenarios.

Authorized licensed use limited to: University of Michigan Library. Downloaded on September 24,2023 at 18:35:06 UTC from IEEE Xplore. Restrictions apply.

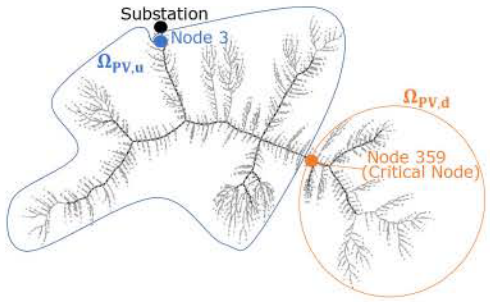

Fig. 4. Taxonomic feeder R1-12.47-1 [37] visualized using [38].

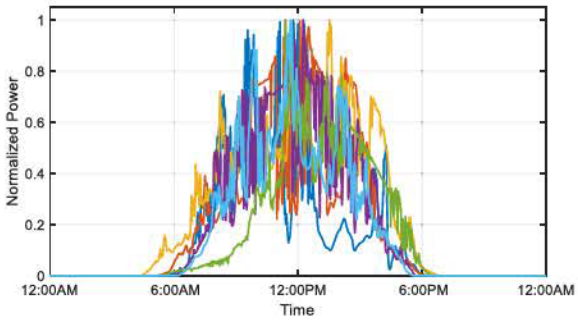

(a) Normalized PV Injections

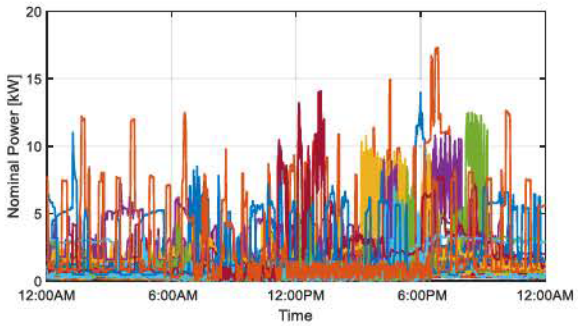

(b) Residential Load

Fig. 5. One-minute resolution measurement data. (a) 6 normalized PV active power injection profiles from NREL [40]. (b) 30 nominal load active power profiles from Pecan Street [41].

A. Feeder Description

We use a large test network based on the R1-12-47-1 taxonomic distribution feeder from Pacific Northwest National Laboratory [37], shown in Fig. 4. It includes 185 three-phase nodes and 1649 single-phase nodes, resulting in $n = 2204$ single-phase connections. We modified the feeder by adding 598 residential solar PV systems (265 connected to phase a, 150 connected to phase b and 183 connected to phase c), all of which belong to Ω_{PV}. Our goal is to minimize voltage unbalance at node-359 (orange dot) where a three-phase motor is connected. It also has a high VUF. We select node-3 to be the proxy critical node (blue dot). The set $\Omega_{PV,d}$ includes 124 PV systems downstream of node-359 (enclosed by the orange line) and $\Omega_{PV,u}$ includes the remaining 474 PV systems (enclosed by the blue line).

B. Simulation Implementation

The optimization-based method was modeled in Julia and the OPF problem was solved using Ipopt [39]. The Steinmetz-based and integrated methods were implemented in MATLAB.

We run two types of simulations to compare the methods. The **static case** models only a single time step and is used to compare computation times and solution qualities. In this case, the integrated method with the direct implementation approach produces the same solution as that of the optimization-based method since it directly uses the results of the optimization-based method in the first time step, and is therefore not included in the comparison. The **time-varying case** models an entire day using load and PV data with 1-minute resolution. The primary purpose of the time-varying case is to investigate the impact of the measurement interval τ_m and time delay τ_d on the performance of all methods. We simulate a benchmark scenario for the optimization-based method in which measurements are available frequently ($\tau_m = 1$ min) and there is no time delay ($\tau_d = 0$). We also simulate two more-realistic scenarios with $\tau_m = \tau_d$ =15 or 60 min. Each variation of the integrated method also uses $\tau_m = \tau_d$ =15 or 60 min. The Steinmetz-based and integrated methods use $\tau_s = 10$ s.

PV active power injections are computed from 1-min irradiance data from the National Renewable Energy Laboratory's Measurement and Instrumentation Data Center [40]. Fig. 5(a) illustrates the six PV generation profiles (from six different cloudy days) used to model the active power injections of PV systems. Each profile is normalized by its maximum value. For each of the PV systems, we scale a randomly assigned normalized profile by a value drawn from a uniform distribution ranging from 9 to 18 kW to obtain its active power injections. We assume the maximum apparent power capacity of each solar PV system is 20 kVA. Additionally, we use 1-min residential load data from Pecan Street [41]. Each of the 598 houses on the feeder is modelled as a ZIP load with nominal active power randomly chosen from one of the 30 24-hour load profiles shown in Fig. 5(b). We assume that load and PV generation remain constant within 1-min intervals.

Defining the PV penetration level as the ratio of the time-varying total PV generation (in kW) to the time-varying total load (in kW), we find that the average PV penetration level throughout the day is 45.63% with a maximum PV penetration of 199.84% occurring at 11:25 am. There is however significant variation in the PV penetration level throughout the day.

C. Performance Metrics

We assess the performance of each method in terms of unbalance improvement and voltage constraint violations.

For the static case, we assess unbalance improvement by reporting the unbalance the critical node VUF_{359} and the mean unbalance across all 185 three-phase nodes, i.e., $VUF_{all} = \sum_{i \in \mathcal{N}_{3\phi}} VUF_i/185$, where $\mathcal{N}_{3\phi}$ is the set of three-phase nodes. As explained in Section III-B, the Steinmetz-based method benefits from an iterative implementation that allows unbalance to converge to a small value. Therefore, all variations of the Steinmetz-based and integrated methods iterate until convergence and we report the results obtained at convergence.

Authorized licensed use limited to: University of Michigan Library. Downloaded on September 24,2023 at 18:35:06 UTC from IEEE Xplore. Restrictions apply.

TABLE III
COMPARISON OF METHODS – STATIC CASE

Method	Unbalance (%) VUF_{359}	Unbalance (%) VUF_{all}	α (%)	Voltage Min (pu)	Voltage Max (pu)
Initial	1.932	1.433	0.000	0.948	1.095
OM	0.001	0.091	0.000	0.913	1.100
SM	0.043	0.063	27.178	0.930	1.142
*SM_{PV}	0.344 (0.114)	0.207 (0.122)	0.000 (27.495)	0.928 (0.927)	1.100 (1.119)
$InDir_{opt}$	0.234	0.135	1.633	0.917	1.135
*$InDir_{opt,PV}$	1.330 (0.720)	0.844 (0.627)	0.045 (20.508)	0.918 (0.911)	1.103 (1.154)
*$InDir_{cons,PV}$	0.248 (0.107)	0.154 (0.115)	0.408 (17.015)	0.922 (0.921)	1.104 (1.115)

*converges to a constant oscillation: peak (trough)

For the time-varying case, we assess unbalance improvement by reporting the mean VUF at the critical node over the day, i.e., $VUF_{359} = \sum_{t\in\mathcal{T}} VUF^t_{359}/T$, where $\mathcal{T}$ is the set of time steps within the simulation and $T = |\mathcal{T}|$ is the number of time steps, with $T = 1440$ for the optimization-based method (corresponding $\tau_m = 1$ min over 24 hours) and $T = 8640$ for the Steinmetz-based and integrated methods (corresponding $\tau_s = 10$ s over 24 hours). We also report the mean VUF across all three-phase nodes and over the day, i.e., $VUF_{all} = \sum_{t\in\mathcal{T}} \sum_{i\in\mathcal{N}_{3\phi}} VUF^t_i/(185 \cdot T)$.

We assess voltage constraint violations by reporting the percent of voltages that violate their voltage limits

$$\alpha = \frac{100}{nT} \sum_{t\in\mathcal{T}} \sum_{i\in\mathcal{N}} \sum_{\phi\in\{a,b,c\}} z_i^{\phi,t}, \tag{25}$$

where $z_i^{\phi,t}$ is a binary variable indicating whether the voltage magnitude in phase ϕ at node i at time step t is outside of the voltage limits, specifically,

$$z_i^{\phi,t} = \begin{cases} 1, & \text{if } |V_i^{\phi,t}| < \underline{V} \text{ or } |V_i^{\phi,t}| > \overline{V} \\ 0, & \text{otherwise,} \end{cases} \tag{26}$$

where $\underline{V} = 0.9$ p.u. and $\overline{V} = 1.1$ p.u. Note that $T = 1$ for the static case. We also report the minimum and maximum p.u. voltage magnitudes across all phases, nodes, and time.

D. Static Case Results

Table III summarizes the static case results computed using load and PV data at 15:15 pm. We observe that the initial VUF at the critical node is close to the 2% IEC Standard limit. Both the optimization-based and Steinmetz-based method significantly reduce the VUF at the critical node, which also leads to considerable reduction in the mean VUF. All variations of the Steinmetz-based and integrated methods use the first heuristic strategy, i.e., a controller at the proxy critical node controls PV systems upstream of the critical node. If we implement SM without this strategy, the VUF at the critical node can only be reduced to 1.008% (versus 0.043%), demonstrating the value of controlling upstream PV systems.

We also see that the optimization-based method produces solutions that do not violate voltage limits (i.e., $\alpha = 0$) but

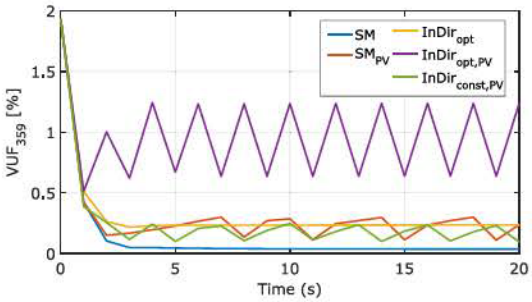

Fig. 6. Convergence of the VUF at the critical node for variations of the Steinmetz-based method and integrated method with the indirect implementation approach. All variations that use the local PV strategy converge to a constant oscillation.

TABLE IV
REACTIVE POWER INJECTIONS (KVAR) OF DOWNSTREAM PV SYSTEMS

Method	Phase a	Phase b	Phase c	Total
OM	-5.97	-422.57	103.16	-325.38
$InDir_{opt}$	220.37	-739.13	193.38	-325.38

the standard Steinmetz-based method results in a large number of overvoltages since it has no mechanism to enforce voltage constraints. Using the local PV strategy, we can reduce the violations at the cost of increasing the VUF. However, the local PV strategy leads to constant oscillations as shown in Fig. 6, where low VUF corresponds to high α and high VUF corresponds to low α. Table III reports results corresponding to the peak and trough of the oscillation.

The integrated method cannot achieve unbalance or voltage results as good as those of the optimization-based method; however, $InDir_{cons,PV}$ has better (average) performance than that of SM_{PV} in terms of both unbalance improvement and voltage constraint violations. Further, $InDir_{opt}$ achieves a comparable unbalance improvement with significantly less voltage constraint violations and no oscillations. Overall, this suggests that setting $\hat{Q}$ equal to the sum of changes in reactive power injections computed by the optimization-based method improves performance.

Despite using the optimization-based method results for $\hat{Q}$ and γ, $InDir_{opt}$ does not have the same performance as the optimization-based method. To explain this, we show the reactive power injections in each phase in Table IV. We see that, though the sum of reactive power injections over all downstream PV systems is the same ($\sum_{k\in\Omega_{PV,d}} Q_{PV,k} = -325.38$ kVAR), the allocation to the phases ($\sum_{k\in\Omega^{\phi}_{PV,d}} Q_{PV,k}\ \forall\phi$) is completely different. Fundamentally, the methods have different goals, with the optimization-based method directly reducing unbalance at the critical node versus the Steinmetz-based method attempting to make the downstream load appear balanced. This is what causes the different phase allocations that, in turn, result in different reactive power set-points and performance.

We next explain why $InDir_{opt,PV}$ performs much worse than $InDir_{const,PV}$, as shown in Fig. 6, despite the only difference being the use of the varying versus constant contribution ratio. Fig. 7 provides a comparison of the γ ratios for all 598 PV

Authorized licensed use limited to: University of Michigan Library. Downloaded on September 24,2023 at 18:35:06 UTC from IEEE Xplore. Restrictions apply.

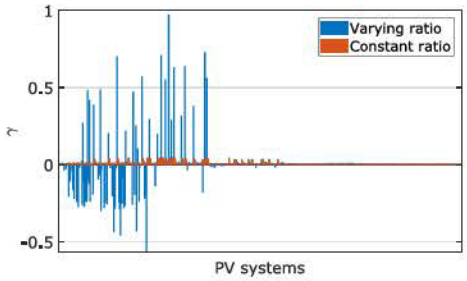

Fig. 7. Comparison between the varying and constant ratios of the integrated method with indirect implementation approach.

systems. As we can see, the varying ratio has much larger absolute values than the constant ratio for some PV systems. The varying ratios can become large when the optimization-based method's reactive power set-points for PV systems on the same phase have different signs but the sum of injections, i.e., the denominator of (21), is small. In our case, the sum of injections on phase a is small (−5.97 kVAR, as reported in Table IV), leading to the large varying ratios shown in Fig. 7. Large ratios lead to large changes in reactive power set-points, which can violate reactive power limits and require modification using (18). When this happens, PV system provide less reactive power compensation than desired, resulting in less unbalance improvement. In our case, the varying ratio causes 90 PV systems to operate at their limits while the constant ratio causes only 22 PV systems to operate at their limits.

Lastly, the integrated method is significantly faster than the optimization-based method. It takes 750 s to solve the optimization problem, but only 0.01 s to solve the linear system of equations used by the Steinmetz-based method, highlighting the benefit of the integrated method, i.e., using the optimization-based method for occasional updates and Steinmetz-based method for frequent updates.

E. Time-Varying Case Results

Table V summarizes the time-varying case results computed using load and PV data from the entire day. Starting with the optimization-based method, we see that the mean VUF and voltage constraint violations increase when the OPF is solved less frequently with longer time delays. The Steinmetz-based method achieves a low mean VUF but voltage constraint violations are significant. Again, the local PV strategy helps reduce voltage constraint violations but increases the VUF. The integrated method with the direct implementation approach performs better than the integrated method with the indirect implementation approach in terms of both unbalance improvement and voltage constraint violations. This means that the set-points generated by the optimization-based method provide a better starting point than the set-points generated by the Steinmetz-based method using the design parameters computed from the set-points generated by the optimization-based method.

We next explore the time-series results of each approach. Fig. 8 compares the time-series results of the optimization-based method (left), Steinmetz-based method (middle), and integrated method with direct implementation approach (right).

TABLE V
COMPARISON OF METHODS – TIME-VARYING CASE

Method	Time (min) τ_m	Time (min) τ_d	Unbalance (%) VUF_{359}	Unbalance (%) VUF_{all}	Voltage α (%)	Voltage Min (pu)	Voltage Max (pu)
Initial	-	-	1.746	1.285	0.087	0.882	1.122
OM	1	0	0.002	0.074	0.000	0.900	1.100
	15	15	0.085	0.108	1.720	0.886	1.134
	60	60	0.174	0.153	2.600	0.897	1.138
SM	-	-	0.043	0.065	17.337	0.916	1.172
SM_{PV}	-	-	0.161	0.122	4.061	0.900	1.138
$InDir_{opt}$	15	15	0.101	0.098	11.613	0.911	1.178
	60	60	0.097	0.094	11.377	0.902	1.164
$InDir_{opt,PV}$	15	15	0.269	0.198	2.325	0.906	1.169
	60	60	0.208	0.159	3.369	0.897	1.163
$InDir_{cons,PV}$	15	15	0.125	0.103	3.008	0.910	1.139
	60	60	0.127	0.103	3.036	0.898	1.143
Dir_{opt}	15	15	0.059	0.092	2.103	0.888	1.146
	60	60	0.093	0.101	4.366	0.872	1.165
$Dir_{opt,PV}$	15	15	0.075	0.098	1.149	0.889	1.160
	60	60	0.106	0.106	1.433	0.876	1.168
$Dir_{cons,PV}$	15	15	0.061	0.092	1.173	0.889	1.134
	60	60	0.100	0.103	1.353	0.875	1.138

The top plots show the evolution of the VUF at the critical node and the bottom plots show the evolution of the maximum and minimum voltage magnitudes across all single-phase connections. The integrated method variations in the right plots all use $\tau_m = \tau_d = 60$ min, and these plots also show the optimization-based method implemented with $\tau_m = \tau_d = 60$ min.

All variations of all methods significantly reduce unbalance at the critical node; however, all but the benchmark (OM with $\tau_m = 1$ min, $\tau_d = 0$ min) lead to over-voltages on phase a, which has the largest number of PV systems, in the middle of the day. Consistent with the results reported in Table V, we can see that unbalance and voltage constraint violations increase when the OPF used by the optimization-based method is solved less frequently. For the Steinmetz-based method, the local PV strategy reduces voltage constraint violations but increases unbalance. Furthermore, while we no longer see *constant* oscillations since the net load is time-varying, the VUF and voltage magnitudes associated with SM_{PV} exhibits high-frequency variation.

Although all variations of the integrated method with the direct implementation approach produce a smaller mean VUF than the optimization-based method implemented with this same measurement interval and time delay (as seen in Table V), in Fig. 8 we can see that there are times when the optimization-based method out-performs the integrated method, for example, during the time period shown in the inset plot. This is because the integrated method tries to maintain the negative-sequence voltage determined by the optimization-based method; however, at such times, if the PV systems were not being actively controlled to change their reactive power injections, the negative-sequence voltage and unbalance would be *decreasing* simply due to changing net load on the feeder. Hence, changes in reactive power set-points generated by the integrated method *increase* unbalance as compared to using

Authorized licensed use limited to: University of Michigan Library. Downloaded on September 24,2023 at 18:35:06 UTC from IEEE Xplore. Restrictions apply.

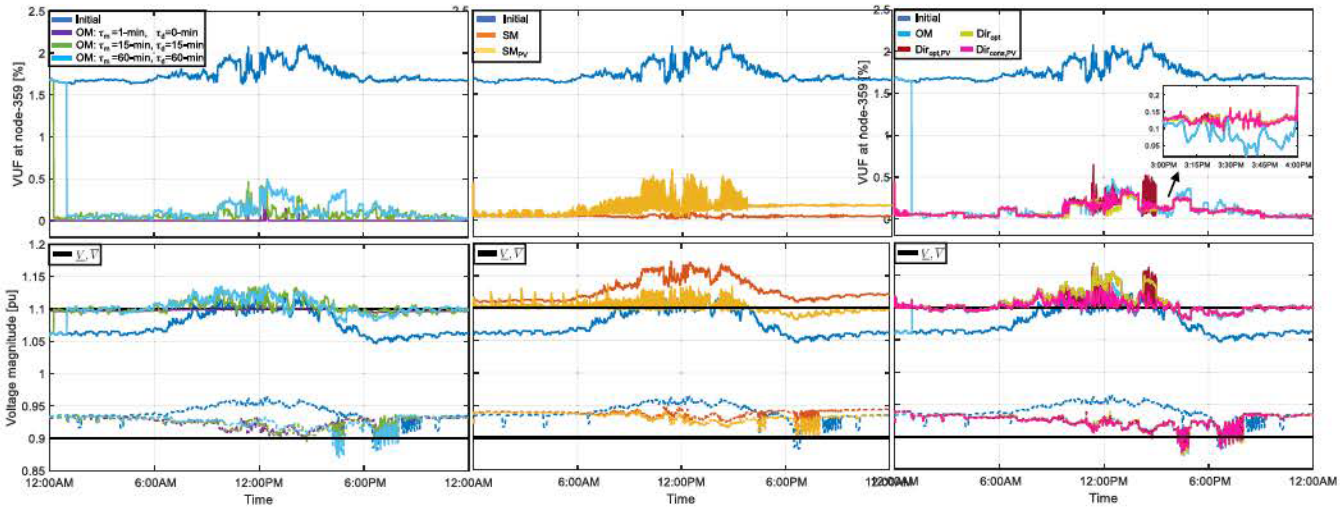

Fig. 8. Comparison of VUF at the critical node and the extreme voltage magnitudes across all single-phase connections for optimization-based (left), Steinmetz-based (middle) and integrated method with direct implementation approach when $\tau_m = \tau_d = 60$-min (right) for the time-varying case. In the bottom three plots, the solid lines are maximum voltage magnitudes and the dashed lines are minimum voltage magnitudes. Solid black lines show the voltage limits.

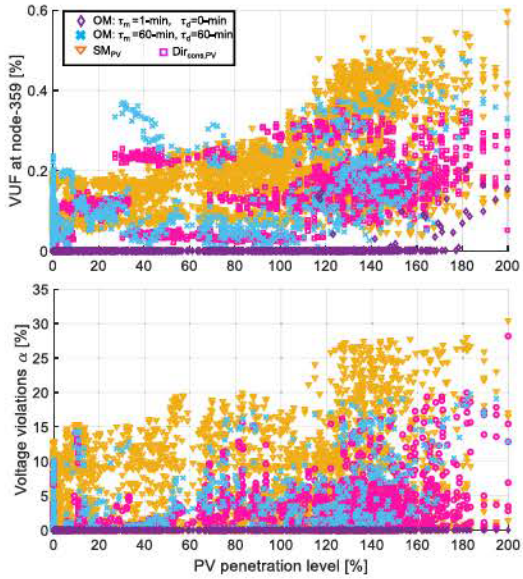

Fig. 9. VUF at critical node-359 (top) and voltage violations at all single-phase connections (bottom) as a function of PV penetration level.

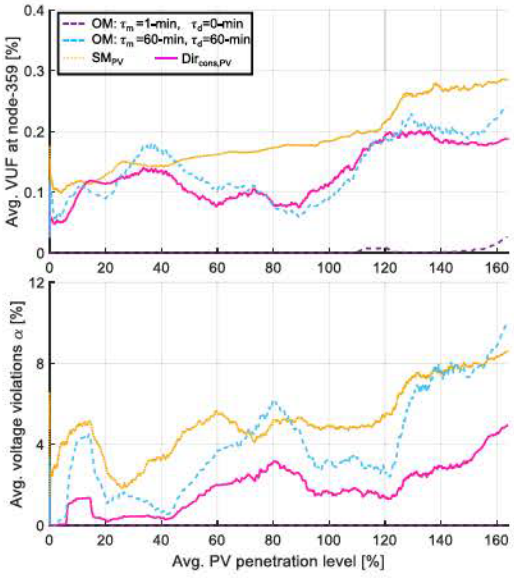

Fig. 10. Smoothed VUF at critical node-359 (top) and voltage violations at all single-phase connections (bottom) as a function of PV penetration level.

the outdated set-points generated by the optimization-based method.

The PV generation and load demand at all 598 houses change significantly throughout the day, resulting in varying PV penetration levels. This allows us to assess how the integrated method performs as the PV penetration level changes. Fig. 9 shows a scatter plot of the VUF at critical node-359 (top) and the percentage of single-phase connections that experience voltage violations (bottom) against the PV penetration level for each of the methods. Although the same PV penetration level can have a range of different VUF and voltage violations, we notice that the VUF and voltage violations tend to increase with higher PV penetration levels. However, the range of the VUF and voltage violations at higher PV penetration levels for the integrated method with direct implementation approach (magenta) is, in general, smaller than the ranges for the optimization-based method (light blue) and Steinmetz-based method (yellow).

To enable a better comparison of the methods, Fig. 10 shows a smoothed version of Fig. 9. Specifically, we compute the averages of both the VUF and voltage violations and plot them against the average of the PV penetration. To compute these averages, we sort the points in order of increasing PV penetration, and create groups with a number of data points corresponding to one hour (i.e., 60 time-steps for the optimization-based method and 360 time-steps for the Steinmetz-based and integrated methods). For each group, we calculate the average PV penetration as well as the average VUF or voltage violations. This figure confirms the above observation that the average VUF and voltage violations increase for higher average PV penetration levels (except for

Authorized licensed use limited to: University of Michigan Library. Downloaded on September 24,2023 at 18:35:06 UTC from IEEE Xplore. Restrictions apply.

TABLE VI
COMPARISON OF METHODS WITH MULTIPLE CRITICAL NODES

Method	Time (min) τ_m	Time (min) τ_d	Unbalance (%) VUF_{five}	Unbalance (%) VUF_{all}	Voltage α (%)
Initial	-	-	1.023	1.285	0.087
OM	1	0	0.006	0.027	0.000
	60	60	0.105	0.140	1.736
SM_{PV}	-	-	0.098	0.133	7.781
$Dir_{cons,PV}$	60	60	0.063	0.089	1.856

the benchmark OM with $\tau_m = 1$ min, $\tau_d = 0$ min). The integrated method with direct implementation approach (magenta) achieves lower average values for VUF and voltage violations even at higher average PV penetration levels compared to the optimization-based (light blue) and Steinmetz-based (yellow) methods.

As mentioned previously, all proposed methods can be extended to consider multiple critical nodes. To investigate this, we consider three additional critical nodes along with node-3 and node-359 and run simulations with the goal to minimize voltage unbalance at all five critical nodes. Table VI summarizes the results obtained using load and PV data from the entire day. We see that all methods are able to considerably reduce the mean VUF across five critical nodes (VUF_{five}). Similar to what we observe in Table V for a single critical node, the Steinmetz-based method achieves a lower average VUF than the optimization-based method (with $\tau_m = \tau_d = 60$ min) but at the expense of more voltage violations. The integrated method with direct implementation approach and local PV strategy ($Dir_{cons,PV}$) provides a compromise between the optimization-based and Steinmetz-based methods; it is able to obtain a lower average VUF than the optimization-based method and fewer voltage violations than the Steinmetz-based method.

V. CONCLUSION

In this paper, we developed a novel approach to reduce voltage unbalance using reactive power injections from single-phase solar PV systems. The new approach combines the advantages of previously developed Steinmetz-based and optimization-based methods to achieve unbalance reduction and manage voltage limits, at reasonable computational and communication burden. The key idea of the method is to use set-points generated occasionally (e.g., every hour) by the high-performing but computationally-expensive optimization-based method to guide the less effective but computationally-simple Steinmetz-based method, which updates the set-points every 10 s. The main contributions of the paper are to investigate different ways in which the two methods can be integrated, and to perform comprehensive experiments to identify drawbacks and benefits of the different approaches. This allows us to provide strong recommendations on how to achieve voltage unbalance reduction with limited computational and communication requirements.

While we acknowledge that the paper does not provide theoretical guarantees for the proposed methods, our main focus was testing these methods by running a comprehensive set of simulations on a large, realistic taxonomic three-phase distribution feeder using time-varying residential load and PV data. Based on our simulation results, we were able to identify the conditions under which the different methods for voltage unbalance mitigation provide or fail to provide good quality solutions. We observed that although the optimization-based method provides the best possible solution, it might not be practical to employ in real systems with limited measurements, network data, and communication infrastructure. In contrast, it is much simpler to implement the Steinmetz-based method but its use can lead to significant voltage constraint violations and/or unbalance and voltage oscillations. The integrated method, if designed correctly, provides a better compromise between performance and information/computational needs. Across all of our experiments, the direct implementation approach provided better results than the indirect implementation approach. Further, using the local PV strategy with the direct implementation approach decreased average voltage constraint violations (at the expense of a small increase in average unbalance). Therefore, we recommend the integrated method with the direct implementation approach and the local PV strategy ($Dir_{cons,PV}$) as the most promising strategy.

Our ongoing and future work is focused on investigating other approximation/relaxation techniques for the optimization-based method to further improve computation time and reduce time delay. We also plan to explore more effective ways of partitioning the PV systems into multiple groups for the Steinmetz-based/integrated methods that achieve better performance. Lastly, we would like to develop robust strategies that further reduce voltage constraints violations when using the integrated method.

REFERENCES

[1] M. Karimi, H. Mokhlis, K. Naidu, S. Uddin, and A. Bakar, "Photovoltaic penetration issues and impacts in distribution network—A review," *Renew. Sustain. Energy Rev.*, vol. 53, pp. 594–605, Jan. 2016.
[2] E. Muljadi, R. Schiferl, and T. Lipo, "Induction machine phase balancing by unsymmetrical thyristor voltage control," *IEEE Trans. Ind. Appl.*, vol. IA-21, no. 3, pp. 669–678, May 1985.
[3] S.-Y. Lee and C.-J. Wu, "On-line reactive power compensation schemes for unbalanced three phase four wire distribution feeders," *IEEE Trans. Power Del.*, vol. 8, no. 4, pp. 1958–1965, Oct. 1993.
[4] Q. Zhang, K. Dehghanpour, and Z. Wang, "Distributed CVR in unbalanced distribution systems with PV penetration," *IEEE Trans. Smart Grid*, vol. 10, no. 5, pp. 5308–5319, Sep. 2019.
[5] Q. Zhang, Y. Guo, Z. Wang, and F. Bu, "Distributed optimal conservation voltage reduction in integrated primary-secondary distribution systems," *IEEE Trans. Smart Grid*, vol. 12, no. 5, pp. 3889–3900, Sep. 2021.
[6] F. A. Viawan and D. Karlsson, "Combined local and remote voltage and reactive power control in the presence of induction machine distributed generation," *IEEE Trans. Power Syst.*, vol. 22, no. 4, pp. 2003–2012, Nov. 2007.
[7] A. R. Malekpour, A. M. Annaswamy, and J. Shah, "Hierarchical hybrid architecture for volt/var control of power distribution grids," *IEEE Trans. Power Syst.*, vol. 35, no. 2, pp. 854–863, Mar. 2020.
[8] X. Su, M. Masoum, and P. Wolfs, "Optimal PV inverter reactive power control and real power curtailment to improve performance of unbalanced four-wire LV distribution networks," *IEEE Trans. Sustain. Energy*, vol. 5, no. 3, pp. 967–977, Jul. 2014.
[9] F. Shahnia, P. Wolfs, and A. Ghosh, "Voltage unbalance reduction in low voltage feeders by dynamic switching of residential customers among three phases," *IEEE Trans. Smart Grid*, vol. 5, no. 3, pp. 1318–1327, May 2014.

Authorized licensed use limited to: University of Michigan Library. Downloaded on September 24,2023 at 18:35:06 UTC from IEEE Xplore. Restrictions apply.

[10] X. Liu, A. Aichhorn, L. Liu, and H. Li, "Coordinated control of distributed energy storage system with tap changer transformers for voltage rise mitigation under high photovoltaic penetration," *IEEE Trans. Smart Grid*, vol. 3, no. 2, pp. 897–906, Jun. 2012.

[11] Y. Xu, L. Tolbert, J. Kueck, and D. Rizy, "Voltage and current unbalance compensation using a static var compensator," *IET Power Electron.*, vol. 3, no. 6, pp. 977–988, 2010.

[12] S. Weckx, C. Gonzalez, and J. Driesen, "Reducing grid losses and voltage unbalance with PV inverters," in *Proc. IEEE Power Energy Soc. Gen. Meeting*, 2014, pp. 1–5.

[13] S. Karagiannopoulos, P. Aristidou, and G. Hug, "A centralised control method for tackling unbalances in active distribution grids," in *Proc. Power Syst. Comput. Conf.*, 2018, pp. 1–7.

[14] K. Schneider et al., "Analytic considerations and design basis for the IEEE distribution test feeders," *IEEE Trans. Power Syst.*, vol. 33, no. 3, pp. 3181–3188, May 2018.

[15] K. Girigoudar and L. Roald, "On the impact of different voltage unbalance metrics in distribution system optimization," *Electr. Power Syst. Res.*, vol. 189, Dec. 2020, Art. no. 106656.

[16] B. A. Robbins and A. D. Domínguez-García, "Optimal reactive power dispatch for voltage regulation in unbalanced distribution systems," *IEEE Trans. Power Syst.*, vol. 31, no. 4, pp. 2903–2913, Jul. 2016.

[17] Q. Peng and S. H. Low, "Distributed optimal power flow algorithm for radial networks, I: Balanced single phase case," *IEEE Trans. Smart Grid*, vol. 9, no. 1, pp. 111–121, Jan. 2018.

[18] B. Zhang, A. Y. Lam, A. D. Domínguez-García, and D. Tse, "An optimal and distributed method for voltage regulation in power distribution systems," *IEEE Trans. Power Syst.*, vol. 30, no. 4, pp. 1714–1726, Jul. 2015.

[19] C. Bajo, S. Hashemi, S. Kjsær, G. Yang, and J. Østergaard, "Voltage unbalance mitigation in LV networks using three-phase PV systems," in *Proc. IEEE Int. Conf. Ind. Technol.*, 2015, pp. 2875–2879.

[20] S. Sun, B. Liang, M. Dong, and J. Taylor, "Phase balancing using energy storage in power grids under uncertainty," *IEEE Trans. Power Syst.*, vol. 31, no. 5, pp. 3891–3903, Sep. 2016.

[21] M. Yao, I. Hiskens, and J. Mathieu, "Mitigating voltage unbalance using distributed solar photovoltaic inverters," *IEEE Trans. Power Syst.*, vol. 36, no. 3, pp. 2642–2651, May 2021.

[22] C. Roberts, S.-T. Ngo, A. Milesi, A. Scaglione, S. Peisert, and D. Arnold, "Deep reinforcement learning for mitigating cyber-physical DER voltage unbalance attacks," in *Proc. Amer. Control Conf.*, 2021, pp. 2861–2867.

[23] O. Jordi, L. Sainz, and M. Chindris, "Steinmetz system design under unbalanced conditions," *Eur. Trans. Electr. Power*, vol. 12, no. 4, pp. 283–290, 2002.

[24] *Electromagnetic Compatibility (EMC)—Environment—Compatibility Levels for Low-Frequency Conducted Disturbances and Signalling in Public Low-Voltage Power Supply Systems*, IEC Standard 61000-2-2, 2018. [Online]. Available: https://webstore.iec.ch/publication/63116

[25] C. Fortescue, "Method of symmetrical co-ordinates applied to the solution of polyphase networks," *Trans. Amer. Inst. Electr. Eng.*, vol. 37, no. 2, pp. 1027–1140, 1918.

[26] A. Siddique, G. Yadava, and B. Singh, "Effects of voltage unbalance on induction motors," in *Proc. IEEE Int. Symp. Electr. Insulat.*, 2004, pp. 26–29.

[27] Y.-J. Wang, "Analysis of effects of three-phase voltage unbalance on induction motors with emphasis on the angle of the complex voltage unbalance factor," *IEEE Trans. Energy Convers.*, vol. 16, no. 3, pp. 270–275, Sep. 2001.

[28] G. A. McCoy and J. G. Douglass, *Premium Efficiency Motor Selection and Application Guide—A Handbook for Industry*, U.S. Dept. Energy, Washington, DC, USA, 2014.

[29] C. Yung, "Stopping a costly leak: The effects of unbalanced voltage on the life and efficiency of three-phase electric motors," U.S. Dept. Energy, Washington, DC, USA, Rep. 200521, 2005. [Online]. Available: http://www.oit.doe.gov/bestpractices/energymatters-/wint2005motors.shmtl, Winter

[30] L. Monjo, L. Sainz, S. Riera, and J. Bergas, "Theoretical study of the Steinmetz circuit design," *Electr. Power Compon. Syst.*, vol. 41, no. 3, pp. 304–323, 2013.

[31] W. H. Kersting, *Distribution System Modeling and Analysis*. Boca Raton, FL, USA: CRC Press, 2006.

[32] M. Bazrafshan and N. Gatsis, "Comprehensive modeling of three-phase distribution systems via the bus admittance matrix," *IEEE Trans. Power Syst.*, vol. 33, no. 2, pp. 2015–2029, Mar. 2018.

[33] A. Wood, B. Wollenberg, and G. Sheblé, *Power Generation, Operation, and Control*. Hoboken, NJ, USA: Wiley, 2013.

[34] Z. Yang, H. Zhong, Q. Xia, A. Bose, and C. Kang, "Optimal power flow based on successive linear approximation of power flow equations," *IET Gener., Transm. Distrib.*, vol. 10, no. 14, pp. 3654–3662, 2016.

[35] S. Geng and I. A. Hiskens, "Convergence of distributed Steinmetz control for balancing distribution network voltages," *IEEE Trans. Power Syst.*, vol. 37, no. 5, pp. 3370–3380, Sep. 2022.

[36] K. Girigoudar and L. A. Roald, "Linearized three-phase optimal power flow models for distribution grids with voltage unbalance," in *Proc. IEEE Conf. Decis. Control*, 2021, pp. 4214–4221.

[37] "GridLAB-D Taxonomy Feeder." PNNL. 2022. [Online]. Available: https://github.com/gridlab-d/Taxonomy_Feeders

[38] "Open modeling framework." NRECA. 2022. [Online]. Available: https://github.com/dpinney/omf

[39] A. Wächter and L. Biegler, "On the implementation of a primal-dual interior point filter line search algorithm for large-scale nonlinear programming," *Math. Program.*, vol. 106, no. 1, pp. 25–57, 2006.

[40] "Measurement and Instrumentation Data Center." NREL. 2022. [Online]. Available: https://midcdmz.nrel.gov/

[41] "Dataport: The world's largest energy data resource." Pecan Street. 2019. [Online]. Available: https://dataport.pecanstreet.org/

Authorized licensed use limited to: University of Michigan Library. Downloaded on September 24,2023 at 18:35:06 UTC from IEEE Xplore. Restrictions apply.